Magnetic anisotropy of monoatomic iron chains embedded in copper

Markus Eisenbach and Balazs L. Györffy
H. H. Wills Physics Laboratory, University of Bristol, Bristol BS8 1TL, United Kingdom

G. Malcolm Stocks and Balazs Újfalussy
Oak Ridge National Laboratory, Oak Ridge, Tennessee 37831-6114
(Received 16 October 2001; published 29 March 2002)

We have calculated the anisotropic magnetic properties of monoatomic chains of iron atoms embedded in fcc copper. The calculations are based on a relativistic extension of the locally self-consistent multiple scattering method that is able to treat the large supercells required to model inhomogeneous systems. We have investigated two chain geometries: Fe chains along the 110 and 100 directions. We found that the magnetocrystalline anisotropy energy favored orientations of the magnetic moments perpendicular to the chains, while the magnetostatic energy was lowest when the moments are aligned parallel to the chain. Interestingly, our parameter free qualitative results implies that these competing effects are finely balanced.

DOI: 10.1103/PhysRevB.65.144424 PACS number(s): 75.75.+a

I. INTRODUCTION

The study of iron inclusions in copper has a long history. Originally systems of iron clusters embedded in a copper matrix were used to study the magnetic properties of γ iron.[1] Recently, interest in such structures has revived due to the observation of giant magneto resistance in these systems[2] and investigation of their magnetic properties has become interesting again.[3] Moreover, progress has been made in fabricating not only randomly distributed clusters but also structures of designed geometries. For example, high-quality iron films can be deposited on or embedded in copper bulk samples.[4] Also individual iron atoms have been positioned on copper substrates to produce well-defined structures such as quantum corrals.[5] Nearer to our interest here, Hauschild *et al.* and Shen *et al.* have been able to deposit chains of individual iron atoms on vicinal surfaces.[6,7] As we have argued previously[8] the balance between magneto crystalline anisotropy and dipolar interaction in one-dimensional systems can give rise to interesting orientational transitions. Clearly, such effects are the one-dimensional analogs of those observed by Allenspach and Bischof[4] in Fe films. In the present work we study iron chains embedded in bulk copper on the basis of first-principles relativistic density functional calculations. Our long term aim is to investigate, with device applications in mind, magnetic structures close to sudden dramatic changes in orientational configuration due to small perturbations, such as a current.[9–11] In this paper we report our discovery and preliminary survey of a rich variety of potentially useful magnetic states of such chains.

In Sec. II we outline a computational framework for treating the relativistic electronic structure problem for a periodic array of atoms with very large unit cells by a real space approach. A previous code in the same spirit as the one presented here was developed by Beiden *et al.*[12] However, their implementation was restricted with respect to the system size that could be treated. As a validation of the method, in the following section, results relevant for bulk bcc iron are presented and compared with those of other calculations. In Sec. IV we present our main results for chains of iron atoms embedded in fcc copper along two different directions. In Sec. V, we discuss the general significance of our findings.

II. RELATIVISTIC LOCALLY SELF-CONSISTENT MULTIPLE SCATTERING METHOD

To perform the calculations for the embedded chains we are employing the first-principles framework of density functional theory in the local spin density approximation (LSDA). We solve the Kohn-Sham equation arising from this formulation of the many body problem by the multiple scattering formalism of Korringa, Kohn, and Rostoker (KKR).[13,14] Since our interest here lies in calculating properties related to magnetocrystalline anisotropy, we have to take into account the coupling between the spin of the electrons and their orbital motion. To do this we utilize relativistic spin density functional theory (Ramana and Rajagopal,[15] MacDonald and Vosko,[16] and Eschrig *et al.*[17]). This leads to solving a Kohn-Sham-Dirac equation of the form

$$[-i\hbar c\vec{\alpha}\cdot\vec{\nabla}+\beta mc^2+V(\vec{r})+\beta\vec{\sigma}\cdot\vec{B}(\vec{r})-E]\psi=0, \quad (1)$$

where $V(\vec{r})$ is the Hartree and exchange correlation electrostatic potential and $\vec{B}(\vec{r})$ is a spin-only exchange field. These relativistic Kohn-Sham-Dirac equations are solved by relativistic spin-polarized version of the KKR method (see Strange[18]).

As usual we render the problem tractable by replacing the infinite sample by a supercell structure—for an ordered system the conventional unit cell; for nonperiod systems some appropriate collection of atoms periodically reproduced. To realistically model inhomogeneous situations of the kind envisioned here, we need to solve the Kohn-Sham-Dirac equation for supercells containing hundreds or even thousands of atomic sites. With present computer technology this is beyond the capability of traditional k space methods. A very effective alternative to this traditional approach has been presented by Wang *et al.*,[19] using an entirely real space formulation of the problem. This latter forms the basis for our relativistic treatment. In short, the locally self-consistent

multiple scattering (LSMS) method of Wang *et al.*[19] is based on the observation that good convergence can be obtained by self-consistently solving the Kohn-Sham equation on a given site by considering not the whole system but only a sufficiently large neighborhood, the local interaction zone (LIZ), about each site. This approach leads to an algorithm that scales linearly in time with the number N of sites in the supercell and, additionally is well suited for implementation on highly parallel computers.[19]

The main quantity we have to calculate in our multiple scattering approach is the scattering path matrix τ, which lets us calculate the Green function on all inequivalent sites in the supercell and therefore many interesting observables. The scattering path matrix $\tau^{ij}_{\Lambda\Lambda'}(\epsilon)$ describes the elastic scattering at energy ϵ via all possible paths of a partial wave with angular momentum indices Λ from site i to a partial wave with angular momentum indices Λ' at site j, where we abbreviate the relativistic angular momentum indices κ and μ with a single label Λ.[18]

To compute the scattering path matrix we need the relativistic structure constants $G^{ij}_{0,\Lambda\Lambda'}$, which are related to the well known nonrelativistic structure constants by

$$G^{ij}_{0,\Lambda\Lambda'}(\epsilon)=\sum_{s=\pm 1/2} C\left(l\frac{1}{2}j;\mu-ss\right) \times G^{ij}_{0,l\mu-sl'\mu'-s}C\left(l'\frac{1}{2}j';\mu'-ss\right), \quad (2)$$

where $C(l\frac{1}{2}j;\mu-ss)$ are the Clebsch-Gordan coefficients and the angular momentum indices l and j are related to κ and μ by

$$l=\begin{cases}\kappa & \text{if} \quad \kappa>0,\\ -\kappa-1 & \text{if} \quad \kappa<0,\end{cases} \quad (3)$$

and $j=l-\frac{1}{2}(\kappa/|\kappa|)$. The second ingredient of MST is the single site t matrix for each atomic sphere of radius R_i assigned to each lattice point $\vec{r}_i$. We calculate the t matrix by numerically integrating the Dirac equation for spherically averaged potentials inside an atomic sphere following the method and approximation described by Feder *et al.*[20] and Strange *et al.*[21] and matching this to the expression for the scattered partial wave in the potential free space. This process, which is described in detail by Strange,[18] yields the single site scattering $t_{\Lambda\Lambda'}(\epsilon)$ for partial waves with angular momentum indices Λ to partial waves with angular momentum indices Λ' at energy ϵ. Note that in the spin polarized relativistic case, as opposed to the spherically symmetric non relativistic case, the single site t matrix is generally no longer diagonal in the angular momentum indices.

The knowledge of t and the free space structure constants G_0 allows us to write the scattering path matrix in real space as a matrix equation

$$\tau=(t^{-1}-G_0)^{-1}, \quad (4)$$

where, following the LSMS approach, $t^{-1}=\{t_i^{-1}\delta_{ij}\}_{ij}$ is a block diagonal matrix containing the single site scattering t matrices, restricted to sites i and j inside a given local interaction zone. (Note that this approximation makes our method an order N method, with N the number of atoms inside a supercell, for a fixed size M of the LIZ. On the other hand, since τ^{-1} is dense the computational effort grows as M^3 as the LIZ size is increased.)

The above formalism then allows us to write the Green function at site i for complex energy ϵ as follows:

$$G^{ii}(\vec{r},\vec{r}';\epsilon)=\sum_{\Lambda_1}\sum_{\Lambda_2} Z_{\Lambda_1}(\vec{r})\tau^{ii}_{\Lambda_1\Lambda_2}(\epsilon)Z^{\dagger}_{\Lambda_2}(\vec{r}') - \sum_{\Lambda} Z_{\Lambda}(\vec{r})J^{\dagger}_{\Lambda}(\vec{r}), \quad (5)$$

where Z and J represent the solutions of the single site Dirac equation.[18] Once the Green function is know the expectation values of ''site diagonal'' operators A_{ii} can be calculated by a trace and an integral along a complex contour ending at the Fermi energy E_f:

$$\langle A\rangle=-\frac{1}{\pi}\mathrm{Im}\int^{E_f}\mathrm{Tr}[A_{ii}(\vec{r},\vec{r}')G^{ii}(\vec{r},\vec{r}';\epsilon)]d\epsilon. \quad (6)$$

The charge and magnetization densities thus obtained then provide us with a starting point for the next iteration step in a selfconsistent calculation, using the local density approximation (LDA) for the exchange-correlation functional.

Frequently, in such calculations the direction of the magnetic moments calculated in an iteration step on a site i will not be parallel to the exchange field, namely, the chosen angular momentum quantization direction $\hat{\mathbf{e}}_i$. To deal with possible noncollinear orientations of the magnetic moments and the local exchange fields, we could assign a local angular momentum and spin quantization axis to each atomic sphere and update this direction in each iteration step to reflect the orientation of the magnetic moment calculated by setting the new direction $\hat{\mathbf{e}}_i^{\mathrm{new}}$ to be a mixture of the original direction $\hat{\mathbf{e}}_i$ and the newly calculated direction $\hat{\mathbf{e}}_i'$ of the magnetic moments, averaged over the atomic sphere Ω_i of radius R_i:

$$\hat{\mathbf{e}}_i'=\frac{\int_{\Omega_i}\vec{m}_i(\vec{r})d^3r}{\left|\int_{\Omega_i}\vec{m}_i(\vec{r})d^3r\right|}. \quad (7)$$

Although one hopes that this procedure will converge to a state where $\hat{\mathbf{e}}_i'$ is along the direction of the exchange field, there is no guarantee that this will happen. Alternatively, we could constrain the magnetic moment inside an atomic sphere to a prescribed direction by requiring that

$$\int_{\Omega_i}\vec{m}(\vec{r})\times\hat{\mathbf{e}}_i d^3r=0. \quad (8)$$

This constraint can be enforced by an auxiliary field as explained by Stocks *et al.*[22] This later approach is the one we adopt for treating the iron moments, whereas we let the di-

TABLE I. The Fermi energy and total energy for bulk bcc iron as function of the local interaction zone (LIZ) size.

LIZ size [sites]	E_{fermi} [Ry]	E_{tot} [Ry]
15 (2 shells)	0.79236	-2522.94226825
27 (3 shells)	0.79465	-2522.94163228
59 (5 shells)	0.78789	-2522.94043070
89 (7 shells)	0.78649	-2522.94072597
113 (8 shells)	0.78778	-2522.94024676
137 (9 shells)	0.78932	-2522.93990050

rection of the magnetic moments of the copper sites evolve according to the first of the two procedures.

III. BULK bcc IRON

In order to validate the above relativistic generalization of the LSMS method of Wang *et al.*[19] we implemented it (RLSMS) for the case of one Fe atom per bcc unit cell and compared the results for the magnetization and magnetic anisotropy energy with those obtained by Beiden *et al.*[12] and by conventional *k*-space calculations as well as experimental results on bulk iron. To illustrate the effect of replacing the Schrödinger equation by a Dirac equation it is useful to record the scattering phase shifts for the iron potential, both for the nonrelativistic and the relativistic case. In the nonrelativistic case the phase shifts are exchange split into two spin channels. This is most obvious for the *d* channel where we find a splitting between the spin up and spin down *d* resonance energies of approximately 0.152 Ry. As expected, in the relativistic case the *d* resonance energies are further split by approximately 0.01 Ry due to spin orbit coupling.

We have calculated, fully self-consistently, the energy and magnetization at a lattice constant of $a=5.27a_0$, corresponding to that of bulk iron. First, the influence of the size of the local interaction zone was tested by calculating the magnetic moments and Fermi energy for different sizes of the LIZ. These results are presented in Table I. The exact result for any system will be reached in the limit $r_{\text{LIZ}} \rightarrow \infty$. Since the computation time grows as M^3, the number M of sites inside the LIZ is proportional to r_{LIZ}^3 for large enough radii, a compromise between accuracy and computation time has to be found. Therefore we have chosen for most of the calculations presented here a LIZ size of 89 sites, or the nearest seven shells of surrounding sites, even though higher accuracy could be achieved at the expense of significantly longer computation time. Furthermore, we have chosen a cutoff in the partial wave expansion of $l_{\max}=3$ for the central site and the two nearest surrounding shells in the LIZ and for the remaining shells we set $l_{\max}=2$. The angular momentum convergence of the KKR method employed by us is discussed in detail by Moghadam *et al.*[23]

With these choices we calculated the magnetic anisotropy for iron as shown in Table II. As can be seen, the spin magnetic moment is in good agreement with previous calculations, both relativistic and nonrelativistic, as well with experimental results. The orbital moment on the other hand is significantly lower in our calculation then it is in the experiment. This deficiency is shared with previous, fully infinite bulk, relativistic calculations. Nevertheless our method produces results for the anisotropy energy of iron that are in reasonable agreement with both experimental and previously calculated results. Thus, we conclude that the magnetic anisotropy energies, calculated in the next section for embedded iron chains, can be taken as realistic quantitative estimates.

IV. IRON CHAINS IN fcc COPPER

We now turn to the central point of our interest, namely, the magnetic anisotropy for chains of single iron atoms embedded in bulk fcc copper. We considered two different geometries. They are depicted in Figs. 1(a) and 1(b), respectively. In all cases we assumed that the lattice constant *a* of copper, which we take to be $6.83a_0$, not to have changed by the iron substitution. The chains in our calculations were chosen to be oriented along the 100 and 110 directions. Note that for the face diagonal case—the 110 direction—two of the nearest neighbors of each iron atom are iron sites again, whereas in the other case all site nearest neighbors to iron sites are occupied by copper and the closest iron atom is on a next nearest neighbor position.

In each fully self-consistent calculation we have determined the total energy, the charge densities on all sites in the unit cell, the size of the magnetization on each Fe atom for a prescribed moment direction, the orientation of the magnetic polarization on the Cu sites and the size of their moments. To determine if the physically preferred orientation of magnetic moments is parallel or perpendicular to the chain direction, we constrained the moment direction on the iron sites to

TABLE II. Magnetic anisotropy energy for bulk bcc iron. The spin and orbital contribution to the magnetic moment associated with an iron site, as well as the the total moment are shown for previous nonrelativistic and relativistic calculations and experiments. The experimental value for the magnetocrystalline anisotropy is listed together with the results from the relativistic calculations.

	μ_{spin}	μ_{orbital}	μ_{total}	$\Delta E_{100,111}$
Non relativistic (Ref. 26)	2.15		2.15	
Relativistic *k* space (Refs. 27,28)	2.08	0.056	2.14	0.07 μRy
Relativistic Beiden *et al.* (Ref. 12)	2.08	0.041	2.13	0.06 μRy
Experiment (Ref. 29)	2.13	0.080	2.21	0.09 μRy
This work	2.13	0.046	2.17	0.06 μRy

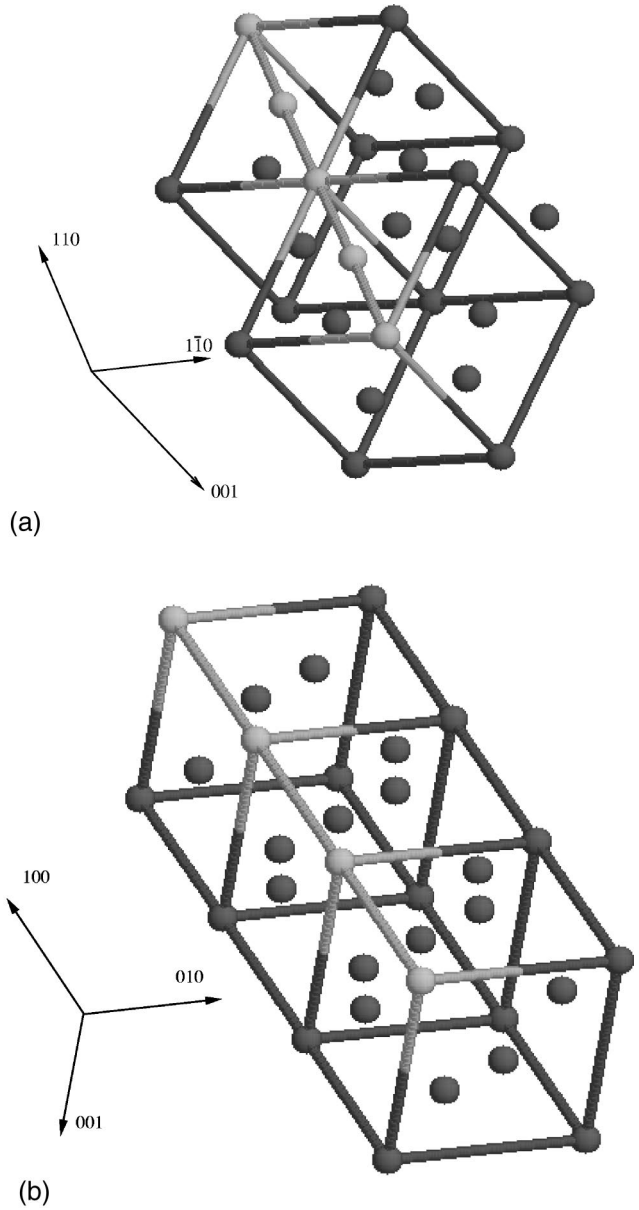

FIG. 1. The orientations of the iron chains in the copper matrix. (a) Chain along the copper 110 direction. Here the iron atoms nearest neighbors. (b) Chain along 100 direction. The pairs of nearest iron atoms have common nearest neighbor copper sites and are next nearest neighbors.

point in a fixed direction and let the moment directions on the copper sites freely fluctuate and converge to their preferred orientation, given the prescribed iron moments. The total number of atoms in the periodically repeated supercell was 16 for the chain oriented along the 100 direction and 12 atoms for the 110 chain. In both cases the cell transverse to the chain axis consisted of one iron site and the remaining sites were occupied by copper, with the supercell oriented in such a way as to align the chain direction with one of the cell edges. A more detailed description of the various unit cells is given in the Appendix.

Since we employ periodic boundary conditions in our calculations, the results we obtain are not for individual chains but for a two-dimensional array of parallel chains. It is therefore necessary to investigate the effect the finite distance between chains has on our results. The results for varying the supercell size for the 110 chain are shown in Table III. The supercells sizes correspond to minimal distances between the iron chains of $2a$, $4a$, and $6a$, respectively. An important benchmark is the size of the induced copper moment on the copper site with the largest distance from the chain. In the ideal case of infinitely separated wires this should vanish in order to correspond to the nonmagnetic bulk copper. Our results suggest that this limit is approached reasonably fast, yet the increase of the supercell size with the chain distance squared introduces a practical limit on the computationally accessible distances.

TABLE III. Effect of the supercell size on μ_{Fe} and μ_{Cu} for the copper furthest from the iron site for the case of the 110 chain.

Supercell size	$\mu_{\mathrm{Fe}}[\mu_B]$	$\mu_{\mathrm{Cu}}[\mu_B]$
12	2.5053	0.0089
48	2.4997	0.0011
108	2.4954	0.0009

In Fig. 2, we show the calculated energy differences between ferromagnetic and antiferromagnetic orderings for the case where the iron moments are oriented along the chain. We note that in both geometries investigated the exchange energy strongly favors the ferromagnetic ordering of the iron spins. This is not at all obvious, even though the iron chain systems are quite different from fcc γ iron, the difference in the local iron environments in the two configurations could have lead to different magnetic ordering.

To investigate the magnetocrystalline anisotropy of the iron chains the total energies have been calculated for ferromagnetic arrangements of the iron moments parallel and perpendicular to the chain directions. The resulting contribution to the anisotropy, given by the difference of these energies, is shown as the left hatched bar in Fig. 3 for each of the chains.

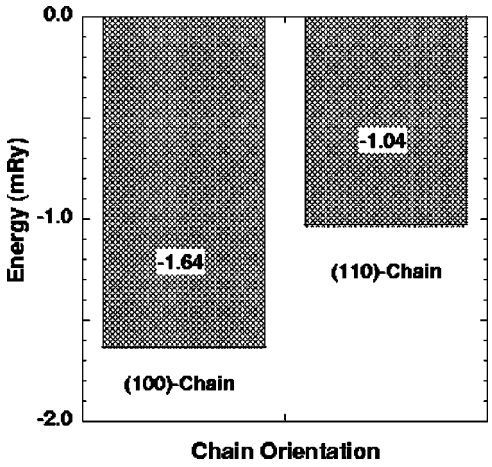

FIG. 2. Stability of the ferromagnetic relative to the antiferromagnetic state. The magnetization is along the wire direction. (Left) Chain along the copper 100 direction. (Right) Chain along the 110 direction.

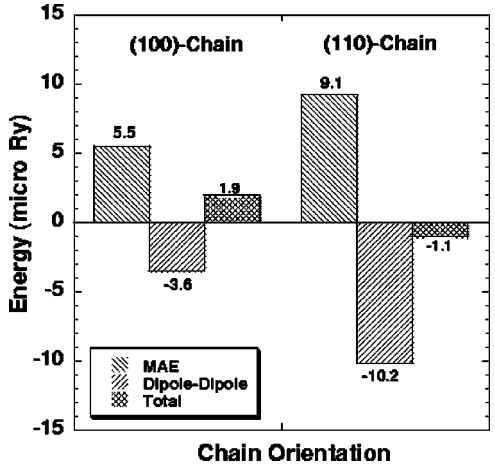

FIG. 3. Total and component anisotropy energies for iron chains in a copper matrix. (Left) Chain along the copper 100 direction. (Right) Chain along the 110 direction.

A positive number in this figure corresponds to a preferential magnetization direction perpendicular to the chain, whereas a negative energy denotes a parallel orientation. Note that to decide which of these orientational configurations is the ground state, we must add to these energies a contribution due to the dipolar interaction between the local moments. This we shall do this presently.

As can be seen from the calculated values for the energy differences in both geometries investigated, the lowest energy state corresponds to the orientation of the magnetic moments on the iron sites perpendicular to the direction of the chains. This is in aggreement with previous model calculations that indicate that the easy direction tends to be perpendicular to the bonds between iron sites.[24,25] In the cases where we studied different orientations transverse to the cluster axis, we found also significant anisotropy associated with the orientation of the iron moments with respect to the copper lattice.

As might have been expected, due to the fact that these systems do not exhibit cubic symmetry, the anisotropy energies per iron atom are significantly higher than that in the cubic bulk sample studied in the previous section. This confirms the widely held belief that the magnetic anisotropy energies of cubic metals are low because in these highly symmetric cases the spin-orbit coupling only makes a contribution to the total energy in fourth order perturbation theory. Presumably, in the present low symmetry arrangement there would be a spin-orbit contribution already to second order. Of course, in our calculations the above statement cannot be made more precise, since the Kohn-Sham-Dirac equation always treats the spin-orbit coupling to all orders.

As mentioned above, the full magnetic contribution to the total energy must include the magnetostatic energy due to the dipolar interaction between the local moments. Even in relativistic LDA calculations this is not part of the theory so far. We shall now add a correction corresponding to this effect. The contribution from the dipolar interaction can be estimated by evaluating the sum for the energy of classical magnetic dipoles

TABLE IV. Magnetic dipolar energy per iron atom for monoatomic chains.

Chain oriented along 100	
Orientation of magnetization	Dipolar energy
FM $\parallel$ chain	$-2.4\ \mu$Ry
AF $\parallel$ chain	$0.9\ \mu$Ry
FM $\perp$ chain	$1.2\ \mu$Ry
Chain oriented along 110	
Orientation of magnetization	Dipolar energy
FM $\parallel$ chain	$-6.8\ \mu$Ry
AF $\parallel$ chain	$2.4\ \mu$Ry
FM $\perp$ chain	$3.4\ \mu$Ry

$$E_{\mathrm{dip}}=\frac{\mu_0}{a^3}\sum_{i\neq j}\left(\frac{\vec{m}_i\cdot\vec{m}_j}{|i-j|^3}-3\frac{m_i^z m_j^z}{|i-j|^3}\right), \tag{9}$$

where we have taken the chain to point along the z direction and a to be the distance between two neighboring dipoles. In the cases we are interested in this sum can easily evaluated and yields the following expressions:[8]

(1) for moments pointing ''head to tail'' (i.e., ferromagnetically) along the z axis

$$E_{\mathrm{dip}}^{\mathrm{FM}}=-4\frac{m^2\mu_0}{a^3}\zeta(3), \tag{10}$$

(2) for the moments pointing in alternating (i.e., antiferromagnetic) directions along the z axis

$$E_{\mathrm{dip}}^{\mathrm{AF}}=\frac{3}{2}\frac{m^2\mu_0}{a^3}\zeta(3), \tag{11}$$

(3) and finally for the magnetic moments perpendicular to the z axis and parallel

$$E_{\mathrm{dip}}^{\perp}=2\frac{m^2\mu_0}{a^3}\zeta(3), \tag{12}$$

where $\zeta(x)$ is the Riemann zeta function, with $\zeta(3)=\Sigma_{i=1}^{\infty}(1/i^3)=1.202057$. The numerical values for the moments obtained in our *ab initio* calculations are shown in Table IV. Clearly, the importance of the magnetic dipolar interaction diminishes rapidly as the distance between the iron sites grows, due to its $1/r^3$ dependence.

The contribution of the magnetostatic dipolar interaction to the magnetic anisotropy of the iron chains can now be obtained by taking the difference of the energies for the ferromagnetic ordering parallel and perpendicular to the chains in Table IV. These values are shown as right hatched bars in Fig. 3. The total magnetic anisotropy is given by the sum of the magnetocrystalline and the magnetostatic contributions, which is represented by the cross hatched bars in Fig. 3. It is readily seen, that, while lowering the energy difference for the 100 chain, the dipolar energy has the potential to change the preferred orientation, so that, in the case of the 110 chain, the lowest energy configuration is that parallel to the chain.

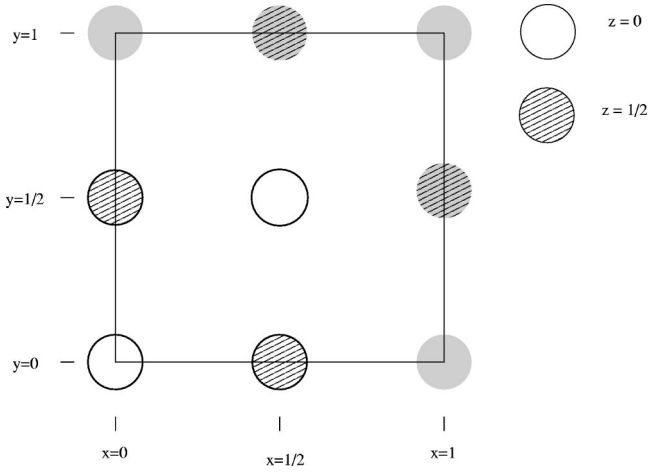

FIG. 4. The fcc unit cell with the 100 direction along the *z* axis. This is the well known four atomic basis for a fcc lattice. The atomic sites belonging to the basis are shown with thick borders, whereas sites already belonging to neighboring cells are marked with a gray background. In addition the *z* coordinate is encoded by the shading of the sites. All coordinates in this and the following figures are given in units of the fcc lattice constant *a*, so that the *x*, *y* and *z* components of the 100 unit cell are unity.

As may be recalled this latter magnetic configuration is what would be expected for a thin magnetized cylinder on the basis of conventional magnetostatics. Evidently, a relatively small perturbation of the 110 chain with a ferromagnetic order along the chain can change the orientation of the magnetization to be perpendicular to the chain axis.

Of course, it has to be noted, that since the iron chains under consideration are one dimensional, one would not expect any long range order at finite temperature in the true thermodynamical sense. Nevertheless experiments on iron stripes at vicinal copper surfaces[7] have observed a hysteresis loop appearing at finite temperatures, thus indicating long timescale magnetic ordering fluctuation in the iron stripes.

V. CONCLUSIONS

We have outlined a method for relativistic first principles DFT calculations in real space, suitable for large supercells. For bulk iron the method gives reasonable agreement with experiments and other calculations based on conventional *k*-space methods for solving the Kohn-Sham-Dirac equation. The main strength of our method lies in its ability to deal with large inhomogeneous systems, as we have shown in the application to monoatomic iron chains embedded in copper. We have shown that the magnitude of the magnetic anisotropy can be controlled by choosing the orientation of the iron chain with respect to the copper lattice. We have yet to investigate further other possible orientations of the iron moments in the chain systems and other arrangements of iron atoms. Evidently one interesting case would be the iron atom corral studied by Crommie *et al.*[5]

ACKNOWLEDGMENTS

This research was supported in part by an appointment (M.E.) to the Postgraduate Research Program at the Oak Ridge National Laboratory administered by the Oak Ridge Institute for Science and Education. Research sponsored by the Division of Materials Sciences and Engineering, Office of Basic Energy Sciences, U.S. Department of Energy, and by the Laboratory Directed Research and Development program of Oak Ridge National Laboratory (ORNL), under Contract No. DE-AC05-00OR22725 with UT-Battelle. The calculations presented in the paper were performed in part at the Center for Computational Sciences (CCS) at ORNL.

APPENDIX: STRUCTURE OF THE UNIT CELLS

Our calculations are aimed at fcc Cu lattices in which the copper atoms along a chosen direction are replaced by iron. To model this with periodically repeated supercells we constructed them in such a way that one edge of the computational cell is aligned with the chain direction. This arrangement of lattice sites is achieved by periodically repeating a generally tetragonal unit cell with a multisite basis with the required fcc lattice direction along the *z* direction of the unit cell. These unit cells, which in the 100 case (Fig. 4) is the well known representation of a face centered cubic lattice by a simple cubic cell with a four atomic basis, are depicted in Figs. 4 and 5. From these unit cells we construct the supercells for the iron chains by repeating the unit cell in the *x* and *y* directions, i.e., the directions perpendicular to the chain. Since our calculations are performed using periodic boundary conditions on the supercell, we effectively calculate arrays of chains and not individual chains. To minimize the effect from this *x*-*y* plane periodicity we need to increase the

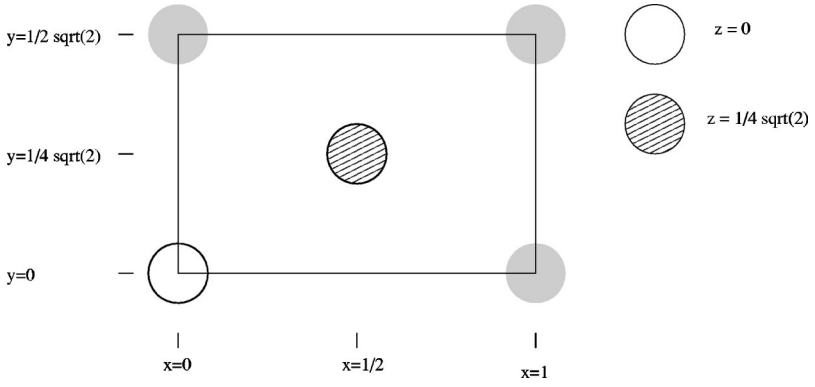

FIG. 5. The 110 unit cell. This is a representation of a fcc unit cell with the *z* axis aligned with the fcc 110 (face diagonal) direction. The basis in this case contains only two atomic sites. The conventions for depicting this cell are the same as chosen for the 100 unit cell in Fig. 4. The *x* dimension is *a*, whereas both the *y* and *z* dimensions of this unit cell are $1/2\sqrt{2}a$.

supercell size in the manner shown in Table III for the 110 chain. To reduce the anisotropy that might be artificially introduced in the system by different distances to the next chain in the x and y direction, we balance the x and y dimension of our supercells as well as possible for a given size. While this is always exactly possible in the case of the 100 unit cell, this balance can be achieved only approximately in the cases of the 110 cell since the unit cell x and y dimensions are not commensurate and it has a x-y unit cell aspect ratio of $1:2\sqrt{2}$. Finally the supercell for our calculation is obtained by stacking this x-y repeat according to the number of nonequivalent iron sites in the chain (i.e., one for ferromagnetic and two for antiferromagnetic ordering) and assigning copper atoms to all lattice sites thus constructed, except for the sites with $x=y=0$ which are occupied by iron atoms.

[1] S. C. Abrahams, L. Guttman, and J. S. Kasper, Phys. Rev. **127**, 2052 (1962).

[2] J. Q. Xiao, J. S. Jiang, and C. L. Chien, Phys. Rev. Lett. **68**, 3749 (1992).

[3] X. Batlle, C. Echer, K. M. Krishnan, B. J. Hattink, and A. Labarta, J. Magn. Magn. Mater. **203**, 120 (1999).

[4] R. Allenspach and A. Bischof, Phys. Rev. Lett. **69**, 3385 (1992).

[5] M. F. Crommie, C. P. Lutz, D. M. Eigler, and E. J. Heller, Surf. Sci. **362**, 864 (1996).

[6] J. Hauschild, H. J. Elmers, and U. Gradmann, Phys. Rev. B **57**, R677 (1998).

[7] J. Shen, R. Skomski, M. Klaua, H. Jenniches, S. S. Manoharan, and J. Kirschner, Phys. Rev. B **56**, 2340 (1997).

[8] M. Eisenbach, M. Dijkstra, and B. L. Györffy, J. Magn. Magn. Mater. **208**, 137 (2000).

[9] J. A. Katine, F. J. Albert, and R. A. Buhrman, Appl. Phys. Lett. **76**, 354 (2000).

[10] J. A. Katine, F. J. Albert, R. A. Buhrman, E. B. Myers, and D. C. Ralph, Phys. Rev. Lett. **84**, 3149 (2000).

[11] K. Bussmann, G. A. Prinz, S.-F. Cheng, and D. Wang, Appl. Phys. Lett. **75**, 2476 (1999).

[12] S. V. Beiden, W. M. Temmerman, Z. Szotek, G. A. Gehring, G. M. Stocks, Y. Wang, D. M. C. Nicholson, W. A. Shelton, and H. Ebert, Phys. Rev. B **57**, 14 247 (1998).

[13] J. Korringa, Physica (Amsterdam) **XIII**, 392 (1947).

[14] W. Kohn and N. Rostoker, Phys. Rev. **94**, 111 (1954).

[15] M. V. Ramana and A. K. Rajagopal, Adv. Chem. Phys. **LIV**, 231 (1983).

[16] A. H. MacDonald and S. H. Vosko, J. Phys. C **12**, 2977 (1979).

[17] H. Eschrig, G. Seifert, and P. Ziesche, Solid State Commun. **56**, 777 (1985).

[18] P. Strange, *Relativistic Quantum Mechanics* (Cambridge University Press, Cambridge, 1998).

[19] Y. Wang, G. M. Stocks, W. A. Shelton, D. M. C. Nicholson, Z. Szotek, and W. M. Temmerman, Phys. Rev. Lett. **75**, 2867 (1995).

[20] R. Feder, F. Rosicky, and B. Ackermann, Z. Phys. B **52**, 31 (1983).

[21] P. Strange, J. Staunton, and B. L. Györffy, J. Phys. C **17**, 3355 (1984).

[22] G. M. Stocks, B. Ujfalussy, X. Wang, D. M. C. Nicholson, W. A. Shelton, Y. Wang, A. Canning, and B. L. Györffy, Philos. Mag. B **78**, 665 (1998).

[23] N. Y. Moghadam, G. M. Stocks, X.-G. Zhang, D. M. C. Nicholson, W. A. Shelton, Y. Wang, and J. S. Faulkner, J. Phys.: Condens. Matter **13**, 3073 (2001).

[24] Ralph Skomski, IEEE Trans. Magn. **34**, 1207 (1998).

[25] Ding-shen Wang, Ruqian Wu, and A. J. Freeman, Phys. Rev. B **47**, 14 932 (1993).

[26] V. L. Moruzzi, J. F. Janak, and A. R. Williams, *Calculated Electronic Properties of Metals* (Pergamon Press, New York, 1978).

[27] H. Ebert, P. Strange, and B. L. Györffy, J. Phys. F **18**, L135 (1988).

[28] S. S. A. Razee, J. B. Staunton, and F. J. Pinski, Phys. Rev. B **56**, 8082 (1997).

[29] *Landolt-Börnstein, New Series*, edited by H. P. J. Wein (Springer-Verlag, Berlin, 1988), Vol. III/19a.